Surface Science 617 (2013) 53–59

Contents lists available at ScienceDirect

Surface Science

journal homepage: www.elsevier.com/locate/susc

Efficient creation and convergence of surface slabs

Wenhao Sun, Gerbrand Ceder *

Department of Materials Science & Engineering, Massachusetts Institute of Technology, Cambridge, MA 02139, USA

ARTICLE INFO

Available online 31 May 2013

Keywords:
Density functional calculations
Surface slabs
Surface slab generation
Surface energy convergence

ABSTRACT

The supercell slab is the structural model used in first-principles simulations to determine thermodynamic, kinetic, and electronic properties of surfaces and interfaces. We present a general algorithm to reorient bulk unit cells using basis and covariant transformations — the first step for constructing surface slabs of any Miller index from bulk unit cells of any Bravais lattice. We further review and discuss subtleties of surface slab creation relevant for performing efficient and accurate calculations of surface properties. We also demonstrate that the nonconvergence of surface energy with respect to slab thickness can be mitigated if the bulk reference energy is calculated from a surface-oriented bulk unit cell, which eliminates Brillouin zone integration errors between the slab and the bulk. Using Pt(111) and Si(111) surfaces as examples, this technique converges the surface energy with respect to slab thickness requiring only one bulk and one relatively thin slab calculation, with moderate *k*-point densities. This process is about an order of magnitude more efficient than popular surface energy convergence techniques involving multiple slab calculations.

1. Introduction

A detailed understanding of surface properties is crucial to many technologies, including catalysis, energy storage, materials synthesis, nanomaterials, as well as to the basic science of surface charge transfer and aqueous stability.[1,2,3] Despite the importance of surface science, experimental determination of surface thermodynamics and electronic structures can be very challenging. For this reason, first-principles calculations of surface properties have become a crucial tool for surface scientists, as they can determine facet-specific surface energies,[4] surface energies as a function of chemical potential,[5,6] nanocrystal morphologies,[7,8] surface electronic structures,[9] charge transfer dynamics,[10,11] work functions,[12] structural reconstructions,[13] interlayer relaxations,[14] adsorbate interactions,[15,16] and more.[17]

The standard structure used to calculate surface properties from first-principles is the surface slab — a supercell representing an infinite two-dimensional thin film oriented to expose the facet of interest, separated from periodic images by a large vacuum. The slab should be thick enough such that there is no interaction between opposite surfaces through the bulk, and the vacuum distance between slabs should be increased until there is no more interaction between adjacent slabs. For a converged, clean slab in vacuum, the surface energy can be defined as

$$\gamma = \frac{1}{2A}\left(E_{slab} - NE_{bulk}\right) \tag{1}$$

where A is the area of the surface unit cell, E_{slab} is the energy of the slab supercell, E_{bulk} is the bulk energy per atom, and N is the number of atoms in the surface slab. The 1/2 pre-factor accounts for the two surfaces of a slab. If the surface can exchange molecular or atomic species with an external reservoir, then the surface grand potential is:

$$\gamma = \frac{1}{2A}\left(E_{slab} - NE_{bulk} - \sum_i N_i\mu_i\right) \tag{2}$$

where excess or deficient atoms are accounted for by a chemical potential term for the N_i atoms of species i with chemical potential μ_i.

Surfaces in realistic environments exist in a variety of physically-relevant configurations, compounding the complexity and cost of a comprehensive theoretical investigation. Nanocrystals usually feature multiple nonequivalent low-energy surface orientations. Each orientation can have multiple terminations, and each termination can potentially be stabilized by a variety of external adsorbates from the chemical environment. A robust and efficient surface generation and calculation scheme can enable a complete exploration of the wide variety of possible surface structures, and is necessary to enable large-scale investigations of material surfaces under realistic conditions.

In this paper, we describe an approach to surface calculations that includes both generalized surface slab creation and rapid surface energy convergence with respect to slab thickness. Along with describing slab creation and convergence, many subtleties of surface calculations are reviewed and discussed. These algorithms are implemented in the open-source Python Materials Genomics (Pymatgen) package,[18] which powers the public first-principles database, The Materials Project.[19] Our analysis of the slab model and slab convergence techniques is also applicable to surface slabs generated from other modeling

* Corresponding author at: 77 Massachusetts Ave, Room 13-5056, Cambridge, MA 02139, USA. Tel.: +1 614 253 1581.
E-mail address: gceder@mit.edu (G. Ceder).

0039-6028/$ – see front matter © 2013 Elsevier B.V. All rights reserved.
http://dx.doi.org/10.1016/j.susc.2013.05.016

tools (including ASE,[20] ACONVASP,[21] Crystal09,[22] GDIS,[23] Materials Studio[24] and METADISE[25]).

2. Generalizing surface slab creation

Surface slabs for the (100), (010), or (001) surfaces of a unit cell can be easily generated by constructing a supercell extended along the [100], [010], or [001] vector, respectively. A vacuum is then added in the same direction and the corresponding atomic coordinates are rescaled appropriately. However, this approach cannot be used to model other surface orientations, as no supercell manipulation of the original unit cell can result in a surface slab consistent both with other orientations of interest and with the periodic boundary conditions.

We present an algorithm to construct surface slabs with any Miller index orientation from a bulk unit cell of any Bravais lattice. The essence of the algorithm is to transform the basis of the bulk unit cell such that the (001) plane of the new basis is oriented parallel to the Miller plane of interest. The transformed basis will therefore have two Bravais lattice vectors, $\mathbf{v}_1$ and $\mathbf{v}_2$, span the plane of the desired surface orientation, and a third Bravais lattice vector, $\mathbf{v}_3$, oriented out of the plane. The atomic positions are then redefined with respect to the new basis using a covariant transformation. Standard surface slab creation procedures can then be performed on the transformed unit cell to prepare a slab structure ready for input into a first-principles calculation package.

2.1. Surface-oriented basis transformation

Surfaces within a crystal are typically defined with respect to the conventional unit cell,[26] using the Miller index notation. Miller notation allows for intuitive visualization of various surfaces (Fig. 1.a), but simulation of surfaces in atomistic codes requires a transformed cell in which the basal plane is coincident with the Miller index of interest (Fig. 1.b).

In order to preserve the Bravais lattice after unit cell transformation, the new basis vectors *must* span Bravais lattice points. The basis vectors $\mathbf{v}_1$ and $\mathbf{v}_2$ are generated from three Bravais lattice points that lie within the desired Miller plane, such that $\mathbf{v}_1 = \mathbf{p}_2 - \mathbf{p}_1$, and $\mathbf{v}_2 = \mathbf{p}_3 - \mathbf{p}_1$. The following is one possible solution for a set of three points corresponding to a given (*hkl*) Miller index. The existence of this solution signifies the completeness of this algorithm in being able to solve for any surface orientation.

For a Miller index containing no zeros, (*hkl*), the following three Bravais points are each collinear to one of the three axes of the conventional unit cell, at a distance corresponding to the reciprocal of their index:

$$\mathbf{p_1} = (\mathrm{M}/h)\mathbf{a}$$
$$\mathbf{p_2} = (\mathrm{M}/k)\mathbf{b}$$
$$\mathbf{p_3} = (\mathrm{M}/l)\mathbf{c}$$

where **a**, **b**, and **c** correspond to the basis vectors of the conventional unit cell, and M is the least common multiple of *h*, *k* and *l*. For example, for the (321) surface, the three points would $\mathbf{p_1} = 2\mathbf{a}$, $\mathbf{p_2} = 3\mathbf{b}$, and $\mathbf{p_3} = 6\mathbf{c}$. Even with primitive cell reduction, high-index surfaces can result in very large two-dimensional surface unit cells.

For a Miller index containing one zero, (*hk*0), these three points can be given with

$$\mathbf{p_1} = (\mathrm{M}/h)\mathbf{a}$$
$$\mathbf{p_2} = (\mathrm{M}/k)\mathbf{b}$$
$$\mathbf{p_3} = \mathbf{p_1} + \mathbf{c}.$$

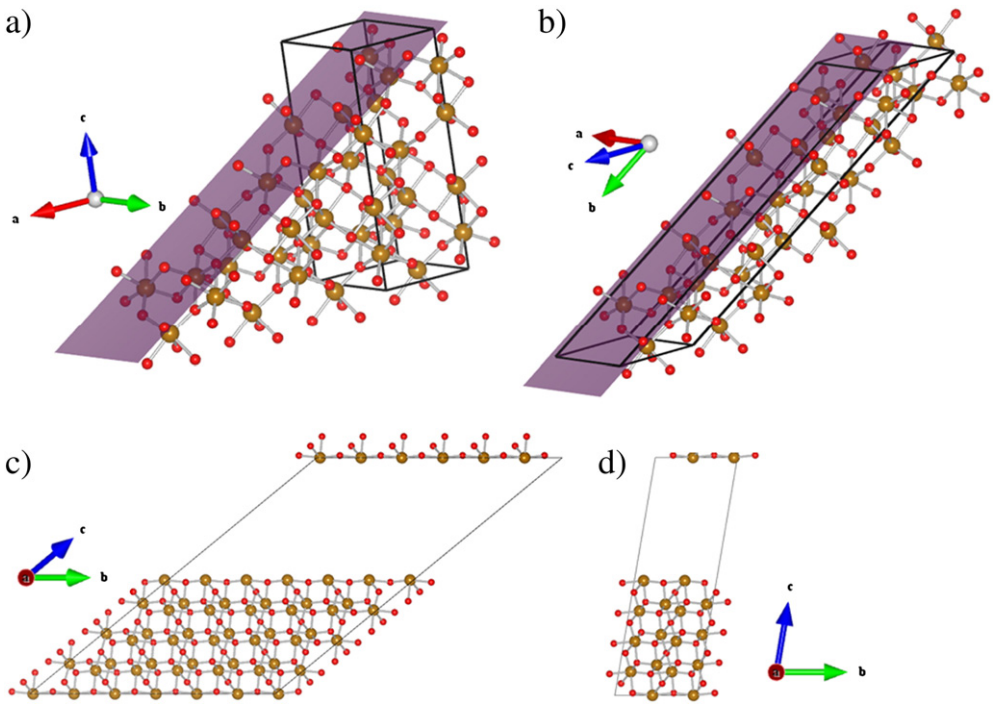

Fig. 1. Constructing the non-polar termination of the $(10\bar{1}4)$ surface of α-Fe_2O_3. a) The $(10\bar{1}4)$ surface is highlighted in the α-Fe_2O_3 crystal structure. b) The bulk unit cell is basis-transformed such that the (001) plane of the new basis is coplanar with the desired $(10\bar{1}4)$ surface. c) The transformed surface-oriented basis is extended using the supercell slab construction to create a six-layer surface slab with a 10 Å vacuum, exposing a non-polar termination. d) The 120 atom slab is reduced by symmetry to the 40 atom primitive surface unit cell. Details of this transformation are described in the Supplementary Information.

And for a Miller index containing two zeros, (h00), these three points can be given as simply

$\mathbf{p_1} = (0,0,0)$
$\mathbf{p_2} = \mathbf{b}$
$\mathbf{p_3} = \mathbf{c}$.

These points for (hk0) and (h00) can be permuted for ($h0l$), (0kl), and (0k0), (00l), as necessary.

These three Bravais points do not represent the minimal possible surface unit cell, but the primitive surface unit cell can be solved from this initial surface slab using unit cell reduction algorithms.[27] This is particularly valuable if a primitive unit cell exists within the bulk conventional unit cell. However, this unit cell reduction is best performed after the complete surface slab is generated, as the vacuum breaks the symmetry perpendicular to the surface, so the primitive cell reduction is correctly confined to only the two dimensions of the surface plane (Fig. 1c–d).

After the two basis vectors in the plane of the surface are determined, a third vector $\mathbf{v}_3$ out of the surface is chosen. This Bravais lattice vector $\mathbf{v}_3$ does not have to be normal to the surface plane, in fact, it can only be normal in the special case that for *any* possible $\mathbf{v}_3$ there exists an integer q such that:

$$(q(\mathbf{v}_3\cdot\mathbf{v}_1))\bmod 1 = (q(\mathbf{v}_3\cdot\mathbf{v}_2))\bmod 1 = 0. \quad (3)$$

This condition can be satisfied for all surfaces in cubic lattices and for hexagonal {100} surfaces, but it is usually impossible to meet in the general case, such as for lower-symmetry Bravais lattices.

That being said, because surface slabs must be thick enough for convergence, it is best that $\mathbf{v}_3$ achieves a maximum slab layer height for a minimal unit cell volume. Therefore, $\mathbf{v}_3$ should be the shortest Bravais lattice vector that is *as orthogonal* to $\mathbf{v}_1$ and $\mathbf{v}_2$ as possible. This choice of $\mathbf{v}_3$ minimizes the total number of atoms necessary for a converged slab, reducing calculation time. A maximally-orthogonal $\mathbf{v}_3$ also minimizes dispersion effects during k-point integration — this is discussed later in the Surface Brillouin zone integration section.

With $\mathbf{v}_1$, $\mathbf{v}_2$, and $\mathbf{v}_3$ determined, the surface-oriented basis transformation is complete: Two basis vectors span the surface with the desired Miller index, and the third basis vector will later be extended with supercell techniques to generate the surface slab. It is best to express the transformed basis such that $\mathbf{v}_1$ and $\mathbf{v}_2$ are in the x–y plane, as it allows for more convenient interpretation of the surface unit cell. This can be done by projecting the three basis vectors onto an orthonormal basis generated around $\mathbf{v}_1$ and $\mathbf{v}_2$ by the Gram–Schmidt procedure.

2.2. Redefining atomic coordinates

The fractional atomic coordinates of the atoms in the system can be redefined with respect to the new surface-oriented basis by use of a covariant transformation. If C is the 3×3 matrix that maps the conventional bulk basis to the surface-oriented basis, such that $S = CB$, where S is the surface-oriented basis, and B is the conventional bulk basis, then the new coordinates A' can be obtained from the old coordinates A with the covariant transformation:

$$A' = \left[\left(C^T\right)^{-1}A^T\right]^T. \quad (4)$$

There are several subtleties to the covariant transformation. The volume of the surface-oriented basis may be an integer multiple of the volume of the original basis, such that a covariant transformation on only the conventional unit cell atoms is not sufficient. One must provide enough atoms to completely fill the transformed basis, and then double-counted atoms and excess atoms outside of the transformed basis should be eliminated.

Also, the transformation must preserve the chemical identity of the elements. An elegant way to perform this operation is by redefining the atomic positions A as an $N\times4$ matrix, such that the fourth column consists of numbers representing chemical identity. Then, C can be the 4×4 matrix, defined such that

$$C = \begin{bmatrix} C_{3\times3} & 0 \\ 0 & 1 \end{bmatrix}. \quad (5)$$

At this point, both the basis and the atoms have been basis transformed with respect to a surface orientation. Several important properties will remain invariant between the original and transformed unit cell: 1) the translational and point-group symmetries, 2) the total energy per formula unit, barring minor numerical integration errors, and 3) the simulated X-ray diffraction pattern. Checking that these properties have not changed is an effective validation of a successful transformation.

We provide a detailed example implementation of the described algorithm to construct the surface-oriented bulk unit cell of the $(10\bar{1}4)$ surface of α-Fe_2O_3 (Fig. 1b) in the Supplementary Information. Also included are 2 MATLAB scripts: 1) to determine a maximally-orthogonal $\mathbf{v}_3$ and 2) to covariantly transform atomic coordinates between bases.

If a transformation is successful, surface slabs can be created from these reoriented bulk unit cells by creating a supercell extended in the [001] direction, and then adding a vacuum in the same direction. The vacuum distance should be extended until the surface property of interest converges. A vacuum length of approximately 10 Å is sufficient for convergence of most surface properties. Converging the thickness of the slab is the subject of the second half of this paper.

With the surface-oriented basis transformation, redefined atomic positions, and relaxed terminations, the surface slab is sufficiently prepared for atomistic simulations. These clean surface slabs can be used to calculate the properties of surfaces in vacuum, and can also serve as template substrates for the interaction of surfaces with a chemical environment.

2.3. Terminations and non-equivalent surfaces

There are usually a number of non-unique termination layers for a given surface orientation. Terminations can be enumerated by placing the origin of the bulk basis at varying positions along $\mathbf{v}_3$, modifying all the fractional z coordinates such that:

$$\text{For } z_0 \text{ in}\{\text{all unique } z \text{ values}\} \;: z_{\text{atom}}{}' = (z_{atom} - z_0)\bmod 1.$$

There is a fundamental challenge in modeling termination-specific surface energies under some crystallographic symmetries. While real surfaces terminate one side of a semi-infinite bulk, surface slab structures are thin-films with a bulk region sandwiched by *two* surface terminations. A tacit assumption from the 1/2 pre-factor in Eq. (1) is that the slab has identical terminations, such that both terminations contribute equally to the resulting surface energy. Unfortunately, identical terminations only occur when the center of the slab has an appropriate symmetry operation, that is, an inversion point symmetry, a 2, 4, or 6-fold rotation axis perpendicular to the slab normal, or a mirror/glide plane parallel to the slab surface.[28] If these required symmetries are not at the center of the slab, then the energy calculated from Eq. (1) is instead the 'cleavage energy', which is the reversible work per area required to separate an infinite bulk along that plane. The cleavage energy is equal to the surface energy when the terminations are identical, but the converse is not necessarily true.

In the case of a solid with charged species, certain terminations can result in a dipole moment in the direction of the vacuum. For example, the stoichiometric MgO (111) surface exhibits alternating charged layers of Mg^{2+} and O^{2-} ions, which forms a polar surface. Under periodic boundary conditions, this electric dipole will lead to a divergence of the electrostatic energy. Tasker has categorized the

surfaces of ionic solids, and for these unstable polar surfaces (also called 'Tasker Type-3 surfaces'), he proposes a workaround to this electric field catastrophe by moving half the charged species on one surface to the other side, effectively removing the electric dipole (resulting in a 'Tasker 2b surface').[29]

Although the Tasker 3 to Tasker 2b reconstruction removes the dipole while preserving stoichiometry, the stability and growth of real polar surfaces is a complicated physical process that might not be best described using this reconstruction. The polar surfaces of strongly ionic rock-salt oxides like MgO (111) facet into a staircase pattern of low-energy {100} surfaces, and for more covalent oxides like NiO, the polar (111) surfaces undergo complicated microfaceting within an octopolar reconstruction.[30] The polar (0001) surface of wurtzite ZnO is electrostatically stabilized by a precise Zn:O surface stoichiometry, achieved by ~30 Å wide, one-layer-high triangular terraces.[31] Molecular crystals with polar building blocks have been shown in Monte Carlo simulations to undergo fundamental growth instabilities, mitigating dipole moments with entropy-driven 180º building block reversals resulting in micro-polarized domains.[32] The dipole can also be mitigated by adsorption of charged species from the environment.[33] These studies suggest that an examination of polar surfaces may be more involved than a Tasker 2b reconstruction.

2.4. Eliminating duplicate orientations and terminations

Identifying families of equivalent surface orientations via crystal symmetry eliminates the need to recalculate duplicate surfaces. Equivalent surface orientations can be determined from the point-group symmetries of a crystal — inversion, rotation, rotoinversion, and mirror planes. Each of these point group operations can be represented by a transformation matrix, but these matrices can only be applied to vectors, and not to Miller indices directly. Therefore, to span a family of equivalent Miller indices, these symmetry operations must be applied to either the surface normal vector of a Miller plane, or to the two surface vectors decomposed from a Miller index, as shown previously. The equivalent Miller indices can then be solved from these transformed vectors, and redundant orientations can be skipped.

Various terminations of the same orientation can also be duplicate. Two terminations can yield trivially identical surface slabs, but two terminations are also identical if they differ from each other by a glide plane or screw axis. The existence of glide planes or screw axes for a given orientation in a crystal can be determined *a priori* from its space group. Surfaces identical through a glide plane, such as the two terminations of the Anatase TiO_2 (100) surface (Fig. 2), can be detected if one slab can be made trivially identical to the other by redefining its origin at another atomic site in its x–y plane. Terminations that are identical through a screw axis can be detected similarly, by first applying a rotation operation to one of the slabs through the axis normal to the x–y plane. Accounting for these coupled translation and rotation symmetries will further eliminate duplicate terminations, saving computation time.

2.5. Relaxation and reconstruction

To alleviate the excess energy of broken bonds, surface atoms tend to relax to more energetically favorable positions. For many solids, this process is a simple compression or expansion of the layers near the surface, known as surface relaxation. It is important to allow for these surface relaxations in atomistic calculations, as surface energy calculations in the literature show that relaxations can reduce the unrelaxed surface energy by approximately 30%. Low-energy electron diffraction data on several metals and ionic compounds suggest that it is usually sufficient to only relax the three outermost surface layers.[34,35,36,37] The remaining atoms in the bulk portion of the surface slab can otherwise be frozen in place to expedite calculation time without affecting the resulting energetics.[38]

The atoms at the surface can also adopt a structure topologically different than the bulk structure, a process known as surface reconstruction. For example, dangling atoms on the Silicon (100) surface will reduce their energy by forming two-atom dimers,[39] with a primitive surface unit cell twice that of the unreconstructed case (a so-called 2×1 reconstruction). Spontaneous reconstruction of clean surfaces can be driven by stress,[40,41,42,43] or can be to restore the lowest-energy electron configuration of the surface species.[44] Adsorption of external molecular and atomic species can also trigger surface reconstruction.[45,46] There are ways to efficiently probe whether a surface has a tendency to reconstruct: imaginary modes in the surface phonon dispersion indicates a driving force for stress-driven reconstruction, and an excess of dangling bonds or unsatisfied atomic orbitals can suggest an electronically-driven surface reconstruction.[47] Actually finding the low-energy reconstructed surfaces involves exploring a broad surface structure-space, and is outside the scope of this paper, although algorithms have been proposed to systematically determine these structures.[48,49]

3. Surface Brillouin zone integration

Due to the unusual geometry of surface slabs under the constraints of periodic boundary conditions, special attention must be paid to the k-space integration of the surface Brillouin zone (SBZ). We present a set of rules regarding choice of k-point grid, integration method, and bulk unit cell orientation, to achieve numerical convergence of surface energies at minimal computational costs.

The k-point grid for surface slabs is generated as $k_1 \times k_2 \times 1$, where the direction with one k-point corresponds to the real-space vector in the direction of the vacuum. Because the SBZ is two dimensional, the energy should be integrated with only one k-point in the direction out of the surface so that there is no dispersion through the vacuum. By definition, k_3 is orthogonal to $\mathbf{v}_1$ and $\mathbf{v}_2$, but this does not require $\mathbf{v}_3$ to be orthogonal to $\mathbf{v}_1$ and $\mathbf{v}_2$. However, if $\mathbf{v}_3$ is not orthogonal to $\mathbf{v}_1$ and $\mathbf{v}_2$, then dispersion effects in the k_1 and k_2 directions are non-zero, but negligible — our calculations show that varying the angle of $\mathbf{v}_3$ versus the surface normal does not change resulting surface energies more than 0.01 J/m^2, which is on the order of numerical integration errors.

Important byproducts of this two-dimensional k-point grid are restrictions placed on Brillouin zone integration. Although the tetrahedron method with Blochl corrections[50] is a standard integration method for insulators and semiconductors, the one k-point in the

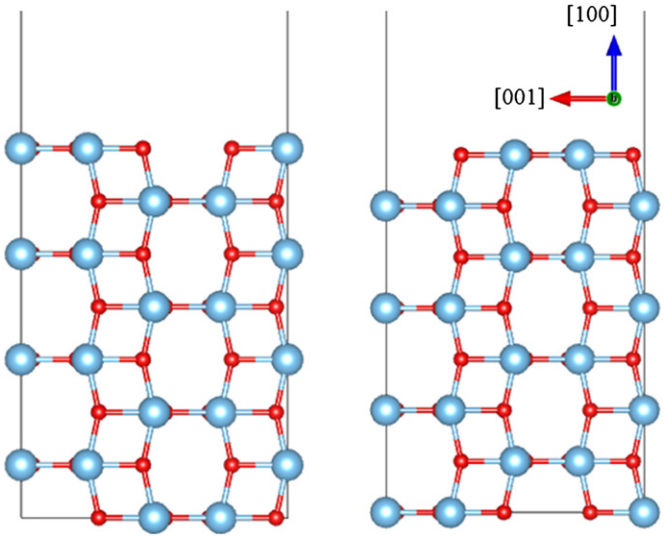

Fig. 2. The two possible terminations of the Anatase TiO_2 (100) surface are identical under periodic boundary conditions by a glide plane translation in the [001] direction.

direction of the vacuum is often inconsistent with the requirements for subdividing the Brillouin zone into tetrahedrons. Therefore, the integration of the surface Brillouin zone is best performed with finite-temperature smearing methods, such as Gaussian smearing or the method of Methfessel–Paxton.[51] An instructive investigation of the smearing parameter can be found in Appendix A of Da Silva et al.[52] One must also be mindful that the *k*-point sampling accurately reflects the reciprocal Bravais lattice of the SBZ — for example, the (111) surfaces of FCC and BCC crystals are hexagonal and require a gamma-centered odd *k*-point grid.

3.1. Consistent k-point integration for rapid slab convergence

As described in the Introduction, the strategy to obtain converged surface slab energies is to increase the vacuum distance between slabs until there is no more interaction between adjacent periodic images, and to increase the slab thickness until there is no interaction between opposite surfaces through the bulk. A peculiar but well-documented phenomenon is that for some surfaces, as the thickness of the slab is increased, the calculated surface energy does not converge. This nonconvergence was first documented by Boettger[53] and was later explored by Fiorentini and Methfessel[54], both sets of authors providing numerical solutions involving multiple slab calculations to circumvent this nonconvergence. Da Silva et al. also addressed this nonconvergence by demonstrating that convergence can be achieved by a single bulk and a single slab calculation using very dense *k*-point grids — from $16 \times 16 \times 1$ up to $32 \times 32 \times 1$.[51] We will show that it is possible to achieve rapidly converged surface energies with a single bulk and a single slab calculation, while maintaining a moderate *k*-point grid.

As observed in the literature, surface energy nonconvergence arises when the well-converged bulk energy is different than the incremental increase of slab energy per layer — e.g. the bulk energy of the surface slab. While the difference between the converged bulk energy and the slab-layer energy may be very small, unless they are identical, the surface energy calculated from Eq. (1) will never converge with thickness.

Boettger proposed a workaround by taking the bulk energy as the difference in energy between a large slab and an incrementally larger slab, by the expression:

$$E_{bulk} = E_{slab}(N+1) - E_{slab}(N) = \Delta E_{slab}/\Delta N \tag{6}$$

where N is the number of layers in the slab. This approach is able to converge on a surface energy with reasonably few slab layers, albeit requiring several slab calculations. However, for numerous systems, the surface energies calculated using the Boettger bulk energy were discovered to oscillate diminishingly around the converged value as the number of layers is increased, due to so-called 'quantum size-effects', requiring relatively thick slabs to have confidently converged surface energies.[55,56,57,58] Fiorentini and Methfessel also popularized a technique to extract the bulk energy involving multiple slab calculations by using a linear relation of the surface slab energy as

$$E_{slab}(N) = 2\gamma + NE_{bulk} \tag{7}$$

and fitting a line through a collection of slab energies, then using the slope of this line as the bulk energy.[58] Both of these techniques are able to improve convergence considerably, however, they are expensive calculations, as they require multiple supercell slab calculations. Finally, Da Silva demonstrates that it is possible to attain converged surface energies simply by resorting to a very dense *k*-point grid,[52] which is also computationally expensive as calculation time scales linearly with the number of *k*-points in the irreducible Brillouin zone.

The fundamental reason why the converged bulk energy can differ from the slab layer energy is because automatically generated *k*-point grids sample the Brillouin zones of the slab and the bulk slightly differently. Integrating the bulk energy from these inconsistent distributions of *k*-points results in the bulk energy difference at the root of surface energy nonconvergence.

One *can* automatically generate the same *k*-point grids for both bulk and surface slabs *by calculating the bulk energy from the surface-oriented basis transformed bulk unit cell*. In this way, the *k*-point sampling of the Brillouin zone in the k_1 and k_2 directions will be identical between the bulk and surface Brillouin zone.

To demonstrate the effectiveness of this approach, we perform calculations on the clean, unrelaxed, unreconstructed Si(111) and Pt(111) surfaces, representing both a semiconductor surface and a free-electron metal surface. The (111) surfaces of cubic crystals are notorious for nonconvergence with respect to the number of layers in the slab, notable examples including Li(111), Al(111), Fe(111), and Co(111).[53] By our reasoning, the cause of the nonconvergence is the three-fold axis along the [111] direction, which results in a hexagonal surface Brillouin zone that is inconsistent with the standard *k*-point sampling of cubic primitive cells.

We prepare the silicon and platinum (111) unit cells using the basis transformation approach described earlier, orienting $\mathbf{v}_1$ and $\mathbf{v}_2$ of the new basis in the (111) plane of the conventional unit cell and choose the [111] direction lattice vector as $\mathbf{v}_3$.

This silicon primitive surface unit cell contains six atoms. For the silicon calculation, the surface slabs start with the primitive unit cell and increase up to sixteen two-atom bilayers (32 atoms). For platinum, the slabs start with the three atom primitive cell, and increase to fifteen atomic layers.

For the hexagonal surface Brillouin zones, we adopt a Gamma-point centered $7 \times 7 \times 1$ *k*-point mesh for the slab calculations. Maintaining *k*-point mesh consistency in the k_1 and k_2 directions between the surface and bulk calculations, we use a $7 \times 7 \times 7$ *k*-point mesh for the bulk calculations. Because the number of atoms per layer is even for the Si(111) case, ideally we would use a $7 \times 7 \times 8$ mesh for the bulk, but this is inconsistent with the Gamma-point centering. This technical limitation results in a minor numerical error.

All calculations were performed using the Vienna Ab-Initio Software Package (VASP). We used the projector augmented wave (PAW)[59] method with the Perdew–Burke–Erzhenhoff (PBE)[60] generalized-gradient approximation. Plane-wave basis cutoff energies were calculated at 125% of the maximum recommended cutoff energy. Brillouin zones were sampled using the Methfessel–Paxton scheme. Bulk unit cells and atoms were initially relaxed until forces were 1E-6 eV/Å. Surface slabs were not relaxed or reconstructed, as the relationship between *k*-point grid and surface energy convergence is not affected by surface structure.

We calculate the bulk energy for Eq. (1) in five ways: 1) as calculated from the primitive bulk unit cells, 2) as calculated from the cubic conventional unit cells (8 atoms for silicon, 4 atoms for platinum), 3) as the difference in slab energy between an N layer and $N + 1$ layer slab (the Boettger relation), 4) the slope of the fitted line between multiple slabs (the Fiorentini and Methfessel relation) and 5) the $7 \times 7 \times 7$ bulk energy from the (111) basis transformed unit cells (this work). These bulk energies are shown in Table 1, and surface energies as a function of the number of layers in the slab are plotted in Fig. 3 for silicon and Fig. 4 for platinum.

We begin with the silicon (111) unreconstructed (1×1) unit cell as a representative model (Fig. 3). There are two non-equivalent terminations for this orientation — we choose the termination with no dangling silicon atoms, which is lower in energy.

Nonconvergence of the surface energy is observed when one uses silicon bulk energies calculated from both the primitive and conventional unit cells, as expected. Although they diverge in opposite directions, it is clear that neither is close to convergence using even a

30-atom thick slab. The most converged relation is the linear-fit scheme by Fiorentini and Methfessel, settling on the value of 1.654 J/m^2 as early as 3 layers. However, this bulk energy was fit to energies from slabs up to 10-bilayer thick. The Boettger bulk energy also calculates a surface energy to be about 1.65 J/m^2, while displaying the characteristic oscillations described previously, although the oscillations are smaller than the DFT error (<0.015 J/m^2). Like the linear-interpolation method, the Boettger method requires multiple slab calculations to achieve the desired convergence.

A single high-density *k*-point calculation is performed, as suggested by Da Silva et al., with a 17 × 17 × 1 grid for a 16 layer surface slab and a 17 × 17 × 17 grid for the primitive bulk cell. This results in a surface energy of 1.652 J/m^2, consistent with the linear fit method, but at a computational cost the same order of magnitude as all twelve slab calculations with 7 × 7 × 1 *k*-point grids. It is not surprising that resorting to an ultra-dense *k*-point grid obviates the numerical integration errors between the bulk and surface Brillouin zones, but it is an unnecessarily expensive solution.

The basis transformed bulk energy calculation proposed in this work is also able to calculate a surface energy of 1.65 J/m^2, using only a 7 × 7 × 7 mesh bulk calculation and a single 7 × 7 × 1 mesh slab calculation. This value is converged for slabs as thin as seven bilayers thick. There is a slight linear nonconvergence of the surface energy, although the surface energy only changes by 0.003 J/m^2 over 10 bilayers. As described earlier, this slight nonconvergence is most likely the result of being unable to use an even number of *k*-points in the k_3 direction. This is the most efficient method listed to achieve the converged surface energy value, requiring an order of magnitude less computation time than the comparably converged linear-fit scheme.

We next turn to platinum (Fig. 4). The surfaces of platinum are particularly well-studied by first-principles calculations, as platinum is an important catalysis material.[61,62] In many ways, the Pt(111) surface behaves similarly to Si(111) with respect to the many convergence schemes. Again, the surface energy does not converge when using a bulk energy calculated from the primitive and conventional bulk unit cells. The Boettger relation surface energy oscillates from quantum size effects, although the oscillations have large amplitudes on the order of 0.4 J/m^2, much greater than for silicon. The amplitude of the oscillations do decrease slightly for $\Delta N = 2$ and $\Delta N = 3$ in the Boettger relation of Eq. (6) (not shown), although they are still greater than 0.2 J/m^2 in amplitude.

The linear-fit method is again successful at converging the surface energy, calculating 1.30 J/m^2 with an error of 0.02 J/m^2 at 7 layers thick, although the bulk energy is fit to slabs with thicknesses from 7 to 14 layers. It is notable that platinum converges with a relatively sparse *k*-point grid, even though metals often need far higher *k*-point densities to achieve convergence of bulk properties. To test the effect of *k*-point density, as per Da Silva et al., the surface energy of Pt(111) was calculated from a 7 layer slab with a 32 × 32 × 1 *k*-point grid, and a primitive bulk unit cell with a 32 × 32 × 32 *k*-point grid, resulting in 1.33 J/m^2. Again, the high *k*-point density method is effective, but costly. Using the (111) basis-transformed bulk energy, the surface energy is converged to 1.31 J/m^2, with an error of 0.02 J/m^2, using only a 3-atom 7 × 7 × 7 mesh bulk calculation and a single 7 × 7 × 1 mesh slab calculation. This value is achieved for slabs as thin as seven atoms thick, again demonstrating that a basis-transformed bulk can achieve rapid convergence at minimal computational cost.

Our calculated surface energy of 1.31 J/m^2 differs slightly from the 1.49 J/m^2 value of Singh-Miller et al. and Chepulskii et al., which also use VASP Projector Augmented Wave psuedopotentials with the PBE pseudopotential. Along with the fact that this study does not include interlayer relaxations, differences can also arise from differences in input parameters, such as the choice of Gaussian smearing and symmetry enforcements of Brillouin zone sampling.

Table 1
Bulk energies of silicon and platinum calculated in a variety of manners. The bulk energy from the Boettger relation oscillates and is not included. The high *k*-point calculations affect the surface slabs more than they affect the bulk calculations, and so high-density bulk calculations are not included here either.

Cell	*k*-point mesh	Bulk eV/atom	
		Silicon (111)	Platinum (111)
Primitive	MP 8 × 8 × 8	−5.41779	−4.1041
Conventional	MP 8 × 8 × 8	−5.42153	−4.1049
Linear-fit	G 7 × 7 × 1	−5.4201	−4.1224
Basis transformed	G 7 × 7 × 7	−5.41976	−4.1247

As presented here, the use of a basis transformed bulk unit cell to obtain the bulk energy for surface energy calculations represents the most computationally efficient way to rapidly achieve converged surface energies, even with moderate *k*-point grids. The root of this success lies in the identical *k*-point integration of the Brillouin zone in the k_1 and k_2 directions for both the slab and the bulk. We also highlight the importance of using odd, gamma-centered hexagonal *k*-point grids for surface Brillouin zones possessing three or six-fold rotational symmetry, such as the (111) surface of cubic crystals. We anticipate that the oversight in making these simple adjustments is the root of much numerical integration error evident in the literature.

4. Conclusion

We have explored a process of constructing surface slab structures that is general across various orientations, crystal structures, terminations and symmetries. The approach is automatable, and a successful implementation enables the unrestricted generation of all potentially relevant surfaces of a material, including the high-index surfaces that are often omitted. Relevant thermodynamic, electronic, and structural properties can then be calculated from these constructed surfaces.

We have further identified that a surface-oriented bulk unit cell has the same 2D surface Brillouin zone as the surface slab constructed from it. By calculating the bulk energy from the basis transformed unit cell, numerical inconsistencies in Brillouin zone integration between the surface slab and bulk are eliminated, resulting in a rapid convergence of surface energy with respect to slab thickness. This convergence is achieved with a single bulk calculation and a single relatively thin slab calculation, using moderate *k*-point densities. This can be an order of magnitude more efficient than other convergence schemes that have been previously proposed.

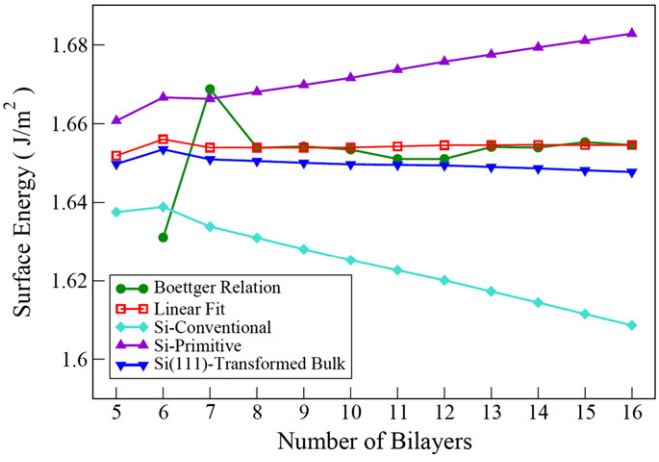

Fig. 3. Surface energies calculated using five different bulk energy values. The silicon (111) transformed basis method is shown to demonstrate rapid convergence at a minimal computation cost of one 7 × 7 × 7 mesh bulk calculation and one 7 × 7 × 1 mesh 16-atomic layer slab calculation.

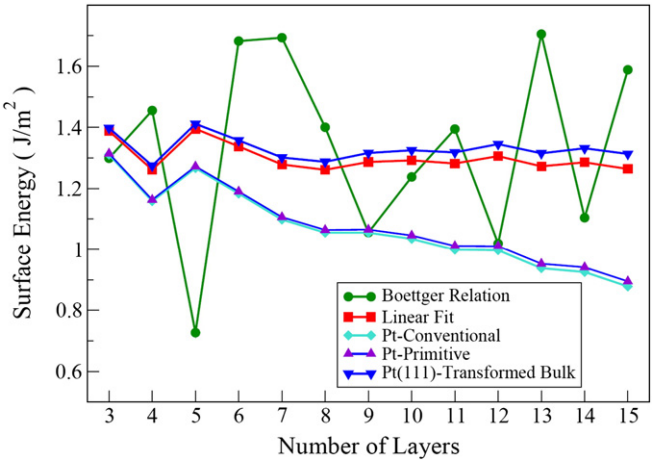

Fig. 4. Platinum (111) surface energies calculated using five different bulk energy values. The platinum (111) transformed basis method is converged within 0.02 J/m^2 at a cost of one $7 \times 7 \times 7$ mesh 3-atom bulk calculation and one $7 \times 7 \times 1$ mesh 7 atomic layer thick slab calculation.

We have thus presented a scheme for the efficient creation and convergence of surface slabs. Combining the generality of the above surface generation algorithm with the efficiency of the rapid convergence scheme enables robust large-scale investigations of surfaces under a variety of realistic conditions.

Acknowledgments

This work was supported by the U.S. Department of Energy, Office of Basic Energy Sciences, under contract No. DE-FG02-96ER45571. Computing resources were provided by the Center for Functional Nanomaterials, Brookhaven National Laboratory, which is supported by the U.S. Department of Energy, Office of Basic Energy Sciences, under Contract No. DE-AC02-98CH10886. WS was also partially supported by the National Science Foundation Graduate Research Fellowship. We further thank Professor Rickard Armiento for helpful discussions.

Appendix A. Supplementary data

Supplementary data to this article can be found online at http://dx.doi.org/10.1016/j.susc.2013.05.016.

Endnotes

[1]Yates Jr, John T., and Charles T. Campbell. *Proceedings of the National Academy of Sciences* 108.3 (2011) 911.
[2]Somorjai, Gabor A., and Yimin Li. *Proceedings of the National Academy of Sciences* 108.3 (2011) 917.
[3]Persson, Kristin A., et al. *Physical Review B* 85.23 (2012) 235438.
[4]Ramamoorthy, Madhavan, David Vanderbilt, and R. D. King-Smith. *Physical Review B* 49.23 (1994) 16721.
[5]Reuter, Karsten, and Matthias Scheffler. *Physical Review B* 65.3 (2001) 035406.
[6]Wang, Xiao-Gang, Anne Chaka, and Matthias Scheffler. *Physical Review Letters* 84.16 (2000) 3650.
[7]Wang, L., et al. *Physical Review B* 76.16 (2007) 165435.
[8]Moll, Nikolaj, et al. *Physical Review B* 54.12 (1996) 8844.
[9]Heifets, E., et al. *Surface science* 513.1 (2002) 211.
[10]Meng, Sheng, and Efthimios Kaxiras. *Nano letters* 10.4 (2010) 1238.
[11]Muiño, R. Díez et al. *Proceedings of the National Academy of Sciences* 108.3 (2011) 971.
[12]Lang, N. D., and W. Kohn. *Physical Review B* 3.4 (1971) 1215.
[13]Brommer, Karl D., et al. *Physical review letters* 68.9 (1992) 1355.
[14]Manassidis, I., A. De Vita, and M. J. Gillan. *Surface science* 285.3 (1993) L517–L521.
[15]Neugebauer, Jörg, and Matthias Scheffler. *Physical Review B* 46.24 (1992) 16067.
[16]Hammer, Bjørk, and Jens Kehlet Nørskov. *Advances in catalysis* 45 (2000) 71.
[17]Nørskov, Jens K., et al. *Proceedings of the National Academy of Sciences* 108.3 (2011) 937.
[18]Ong, Shyue Ping, et al. *Computational Materials Science* 68 (2013) 314.
[19]S. P. Ong, A. Jain, G. Hautier, M. Kocher, S. Cholia, D. Gunter, D. Bailey, D. Skinner, K. Persson, G. Ceder, The Materials Project. http://materialsproject.org/.
[20]S. R. Bahn and K. W. Jacobsen, Comput. Sci. Eng. 4 (2002) 56.
[21]S. Curtarolo, W. Setyawan, G. L. W. Hart, M. Jahnatek, R. V. Chepulskii, R. H. Taylor, S. Wang, J. Xue, K. Yang, O. Levy, M. Mehl, H. T. Stokes, D. O. Demchenko, and D. Morgan, Comp. Mat. Sci. 58 (2012) 218.
[22]Dovesi, Roberto, et al. Zeitschrift für Kristallographie 220.5/6/2005 (2005) 571.
[23]Sean Fleming* and Andrew Rohl, Z. Kristallogr. 220 (2005) 580.
[24]Materials Studio is a product of Accelrys, Inc., San Diego, CA.
[25]G.W. Watson, E. T. Kelsey, N. H. deLeeuw, D. J. Harris and S. C. Parker, Journal of the Chemical Society-Faraday Transactions 92 (1996) 433.
[26]Parthé, E., and L. M. Gelato. *Acta Crystallographica Section A: Foundations of Crystallography* 40.3 (1984) 169.
[27]Buerger, M. J. *Zeitschrift für Kristallographie* 109.1 (1957) 42.Santoro, A. T., and A. D. Mighell. *Acta Crystallographica Section A: Crystal Physics, Diffraction, Theoretical and General Crystallography* 26.1 (1970) 124.
[28]Even when the necessary symmetry elements exist for a given orientation, if they are not at the center of the slab, there is no clever reconstruction of slab such that the two surfaces can exhibit identical terminations without being inconsistent Eq. (1). If one parses the non-symmetric slab into two portions — one above the necessary point-symmetry and one below, then performs the symmetry operation to generate a slab with identical top and bottom, the number of atoms in the two new slabs will not necessarily be an integer multiple of the number of atoms in the bulk unit cell. One would thus be unable to subtract away the bulk energy from this slab using Eq. (1).
[29]Tasker, P. W. *Journal of Physics C: Solid State Physics* 12.22 (2001) 4977.
[30]Noguera, Claudine. *Journal of Physics: Condensed Matter* 12.31 (2000) R367.
[31]Dulub, Olga, Ulrike Diebold, and G. Kresse. "*Physical review letters* 90.1 (2003) 16102.
[32]Hulliger, Jürg, et al. *Crystal Growth & Design*.
[33]Rohr, F., et al. *Surface science* 315.1 (1994) L977.
[34]Lindgren, S. Å. et al. *Physical Review B* 29.2 (1984) 576.
[35]Tian, Lan and X.U. Fei-Yue. "A study of GaAs (110) surface relaxation with low-energy-electron-diffraction." (2005) 357.
[36]Ferry, D. et al. *Journal of Vacuum Science & Technology A: Vacuum, Surfaces, and Films* 16.4 (1998) 2261.
[37]Li, Y. S. et al. *Physical Review B* 40.12 (1989) 8239.
[38]Hameeuw, K. J. et al. *The Journal of chemical physics* 124 (2006) 024708.
[39]Chadi, D. J. *Physical Review Letters* 43.1 (1979) 43.
[40]Fiorentini, Vincenzo, Michael Methfessel, and Matthias Scheffler. *Physical review letters* 71.7 (1993) 1051.
[41]Wan, Jun, et al. *Modelling and Simulation in Materials Science and Engineering* 7.2 (1999) 189.
[42]Needs, R. J., M. J. Godfrey, and M. Mansfield. *Surface Science* 242.1 (1991) 215.
[43]Lazzeri, Michele, and Annabella Selloni. *Physical review letters* 87.26 (2001) 266105.
[44]Pandey, K. C. *Physica B + C*117 (1983) 761.
[45]Jacobsen, K. W., and J. K. Nørskov. *Physical review letters* 60.24 (1988) 2496.
[46]Germer, L. H., and A. U. MacRae. *Proceedings of the National Academy of Sciences of the United States of America* 48.6 (1962) 997.
[47]Srivastava, G. P. *Reports on Progress in Physics* 60.5 (1999) 561.
[48]F. C. Chuang, C. V. Ciobanu, V. B. Shenoy, C. Z. Wang, and K. M. Ho. Surf. Sci., 573 (2004) L375.
[49]Thomas, John C., et al. *Physical Review B* 82.16 (2010) 165434.
[50]Blöchl, Peter E., O. Jepsen, and O. K. Andersen. *Physical Review B* 49.23 (1994) 16223.
[51]Methfessel, M. P. A. T., and A. T. Paxton. *Physical Review B* 40.6 (1989) 3616.
[52]Da Silva, Juarez LF, Catherine Stampfl, and Matthias Scheffler. *Surface Science* 600.3 (2006) 703.
[53]Boettger, J. C. *Physical Review B* 49 (1994) 1472907.
[54]Fiorentini, Vincenzo, and M. Methfessel. *Journal of Physics: Condensed Matter* 8.36 (1996) 6525.
[55]Kiejna, A., J. Peisert, and P. Scharoch. *Surface science* 432.1 (1999) 54.
[56]Wei, C. M., and M. Y. Chou. *Physical Review B* 66.23 (2002) 233408.
[57]Sun, Bo, et al. *Physical Review B* 75.24 (2007) 245422.
[58]Gay, J. G. et al. *Journal of Vacuum Science & Technology A: Vacuum, Surfaces, and Films* 2.2 (1984) 931.
[59]Blöchl, Peter E., O. Jepsen, and O. K. Andersen. *Physical Review B* 49.23 (1994) 16223.
[60]Perdew, John P., Kieron Burke, and Matthias Ernzerhof. *Physical review letters* 77.18 (1996) 3865.
[61]Singh-Miller, Nicholas E., and Nicola Marzari. *Physical Review B* 80.23 (2009) 235407.
[62]Chepulskii, Roman V., and Stefano Curtarolo. *ACS nano* 5.1 (2010) 247.